Int. J. Therm. Sci. (2001) 40, 517–527

S1290-0729(01)01240-6/FLA

Solution of the radiative transfer equation in discrete ordinate form by sequential function approximation

David L. Thomson, Andrew J. Meade, Jr. *, Yildiz Bayazitoglu

Department of Mechanical Engineering and Materials Science, William Marsh Rice University, 6100 Main St., Houston, TX 77005-1892, USA

(Received 6 March 2000, accepted 7 December 2000)

Abstract — An adaptive and scalable alternative to the finite element and finite volume methods is developed to solve the steady multi-dimensional radiative transport equation. Solutions to the problem of heat transfer within a two-dimensional box through a non-scattering medium are presented and compared to the results from popular finite volume methods. The accuracy level of the developed method, using skewed piecewise linear bases, surpasses that of the finite volume results using the popular step and diamond schemes on a regular grid. Moreover, the accuracy levels are achieved with less than 1 % of the number of control volumes used by the finite volume methods. © 2001 Éditions scientifiques et médicales Elsevier SAS

radiative heat transfer / adaptive computing / optimization

Nomenclature

A	numerator in coefficient equation
$\mathcal{B}$	linear boundary operator
B	denominator in coefficient equation
C_δ	positive constant
c_d^k	kth coefficient in the SFA method for a discrete ordinate
D	number of ordinate directions
G	incident radiation
g	forcing function
H	Hilbert space
h	grid spacing
$\mathbf{I}$	intensity of radiation numerical vector
I	intensity of radiation
I_b	black body intensity of radiation (Planck function)
$\mathcal{L}$	linear differential operator
L	distance between parallel plates
N	number of bases
n_p	number of basis parameters
p	polynomial order of basis function
$\mathbf{Q}$	vector of optimization constraints
q	heat flux scalar
$\mathbf{R}$	equation residual vector
$\mathbf{r}$	position vector
S_n	angular quadrature scheme
T	temperature (K)
w_d	quadrature weight for a discrete ordinate
x	spatial coordinate
y	spatial coordinate
$\langle\cdot,\cdot\rangle$	inner product

Greek symbols

β	extinction coefficient
δ	Kronecker delta
ε	emissivity of a surface
ε_r	solution error/small positive number
η	local coordinate of basis function in the x direction
θ_x	angle between the η and x axes
θ_y	angle between the ξ and y axes
Λ	objective function
ξ	local coordinate of basis function in the y direction
σ	Stefan–Boltzmann constant $= 5.67{\cdot}10^{-8}$ . . . . . $\mathrm{W{\cdot}m^{-2}{\cdot}K^{-4}}$
ϕ	weighting function
ψ	basis function
Ω	solid angle . . . . . rad
Ω_{dn}	direction cosine to the hypothetical surface normal vector

* Correspondence and reprints.
E-mail address: meade@rice.edu (A.J. Meade).

Subscripts

B	belonging to the boundary
$\mathcal{B}$	belonging to the boundary equation
d	dummy index/associated with a discrete ordinate
i	dummy index
j	dummy index
$\mathcal{L}$	belonging to the differential equation
L	basis parameter
l	dummy index
lin	belonging to the piecewise linear basis
M	basis parameter
n	dummy index
p	dummy index
R	basis parameter
skewed	belonging to the piecewise linear skewed basis
x	x direction
y	y direction

Superscripts

j	dummy index
k	dummy index
m	order of a Hilbert space norm
s	order of a Hilbert space norm
γ	order of convergence defined in equation (1)
ζ	dimension of the problem domain
$\tilde{}$	approximation

1. INTRODUCTION

The resulting integro-differential equation makes solution techniques to radiation heat transfer problems fundamentally different from those of conduction and convection. The speedy, accurate, and computationally efficient solution of the radiative transfer equation (RTE) is of considerable importance in engineering in order to solve multidimensional problems. Howell [1] suggested that parallel Monte Carlo techniques [2] should be efficient in solving the integro-differential equation for any number of processors since interprocessor communication is not needed between individual "games". Novo et al. [3] attempted to parallelize the radiative transport equation through an angular decomposition method known as the discrete ordinate method (DOM) [4, 5]. In the DOM, integrals over the solid angular domain in the RTE are approximated by a quadrature rule over discrete directions, where an appropriate quadrature set is chosen [6] based on the scattering function used. Novo et al. noticed that the angular domain is readily parallelized with high efficiencies, as verified by Haferman et al. [7], since each direction may be calculated independently for a given radiative source. Using the finite element method (FEM) on the discrete ordinate form of the RTE (DOM/RTE), Burns [8] introduced a parallel sparse iterative solver in the spatial domain.

An additional difficulty in the DOM/RTE presents itself in multiple dimensions and that is the possible presence of non-physical discontinuities in the DOM formulation, commonly known as "ray effects" [9]. Three techniques have proven successful in the literature in reducing the ray effect. The first and most common technique is simply to increase the number of ordinate directions. This has the effect of increasing the actual number of discontinuities while reducing the respective magnitudes of each. The second technique is the use of alternative quadrature sets for certain types of problem. The third technique is to use the numerical method itself to smooth the non-physical artifacts of the DOM by the use of "false scattering", as described by Chai et al. [9]. An additional, or fourth, approach not found in the literature is the use of a user-defined or physically consistent smoothing technique similar to the use of artifical viscosity and entropy in computational fluid dynamics [10].

There are problems associated with each of the four techniques. The first technique merely increases the problem size and defeats the purpose of the DOM and the numerical method. The second technique is problem specific and may not be useful for general problems. In the third technique, the numerical smoothing is a result of an inaccurate solution of the DOM/RTE. It is, therefore, grid dependent and so may be difficult to reproduce. A slight change in a course grid will affect the solution profile noticeably, and an increasingly finer grid will produce an accurate and discontinuous solution. The physically consistent formulation of the fourth technique is not yet available, and the user-defined technique may be problem specific. However, the user-defined artificial scattering would at least be reproducible.

In the present work, an optimal solution algorithm is developed based on sequential function approximation (SFA) for the multi-dimensional DOM/RTE without the "ray effects". It is a user-friendly, solution-adaptive, and matrix-free automatic "meshless" solver algorithm that we also believe has the potential to utilize parallelism in the spatial domain. Results for heat transfer within a two-dimensional black box through non-scattering media are given and compared with popular finite volume method (FVM) schemes on a regular grid.

2. SOLUTION PROCEDURE

In this section we will outline the FVM approach and the adaptive approximation of differential equations. This is followed by a discussion of the SFA method which will be used to approximate the solution to the RTE, optimization methods, and the local basis functions to be used in the approximations.

2.1. Finite volume solutions of RTE by DOM

In a typical application of the finite volume method to the DOM, the problem domain is divided into a mesh of regular control volumes (CVs) corresponding to the boundaries of the domain and oriented with respect to the chosen coordinate system.

The two most popular FVM schemes applied to the DOM/RTE are the diamond and step. In the diamond scheme the cell center value can be chosen as a simple average. This choice however, can result in oscillatory solutions throughout the domain and nearly always includes overshoots and undershoots near the location of a discontinuity. Also, the oscillations decrease with an increasingly fine mesh but they do not vanish. The scheme does, however, capture the locations of discontinuities with fewer grid points than its alternative, the step scheme.

The step scheme is effective in removing the oscillations generated by the discontinuities. In addition, the discontinuity, which is a non-physical artifact of the DOM, is removed as well through the addition of false scattering. In fact, many consider the step scheme to produce better solutions than the diamond scheme since the actual physical solution does not possess discontinuities. Because the solution is basically incorrect it is also very grid sensitive. As the grid grows finer the solution exhibits the expected DOM generated discontinuities.

These deficiencies suggest that neither of these FVM schemes is completely satisfactory with current DOM angular discretizations. We offer the sequential function approximation method as an alternative. The SFA method to be used in this work is based on a variety of techniques borrowed from various subdisciplines in computational mechanics. First developed in artificial neural networks research, the SFA method has been employed for iterative function approximation. Motivated by similarities observed in adaptive grid optimization techniques in the solution of partial differential equations (PDEs), Meade et al. [11] reformulated the SFA method with the help of the closely related method of weighted residuals. To begin our discussion on the SFA method, we must first outline adaptive grid optimization.

2.2. Adaptive grid optimization

The purpose of all adaptive grid techniques is to generate an optimal node distribution based on some objective. The common characteristic of these techniques is that a grid is generated and a solution found. Diaz et al. [12] classified their optimal node distribution as a relocation technique, or r method, including it among the well-known h, p, and h–p adaptive methods. Using error analysis from finite elements [13], we can write

$$\|\varepsilon_r\|_{H^m} \le C_\delta h^\gamma \|I_d\|_{H^s} \approx C_\delta N^{-\gamma/\zeta} \|I_d\|_{H^s} \quad \text{and}$$
$$\gamma = \min(p+1-m, s-m) \tag{1}$$

In h methods the quality of the solution is improved by reducing the grid spacing h with the introduction of additional basis functions. In p methods, the polynomial order of the basis functions, p, is increased, while h–p methods combine the introduction of additional basis functions with an increase in the order of existing and/or introduced bases. In the r method, the locations of the grid nodes, i.e., the locations of the basis functions, are adjusted to increase the accuracy and consequently to decrease the value of the constant C_δ.

It is well known that most of the computational time required by codes that utilize adaptive techniques is spent on the required grid generation [14]. Reference [15] stated that the major challenges to adaptive methods in computational mechanics include:

1. The use of unstructured meshes and their resulting elaborate and complicated data structures.
2. The necessity of explicit or iterative solution techniques due to the poor performance of direct solvers on dynamically evolving unstructured meshes.
3. Stability issues of the associated numerical schemes stemming from the continuous changes in the data structures and polynomial order of the bases.
4. The computational overhead of the error estimation and the adaptation process.

The SFA method presented in this paper features the advantages of adaptive methods without sharing their disadvantages.

2.3. Application of the proposed SFA method

In the SFA method, as an alternative to the conventional FVM and FE approaches, an incremental set of interpolation functions is built sequentially by an optimization method to improve the expansion-based approximation. The function at any step k is approximated as [11]

$$\widetilde{I}_d^k(\mathbf{r}) = \widetilde{I}_d^{k-1}(\mathbf{r}) + c_d^k \psi_d^k(\mathbf{r}) \tag{2}$$

Therefore, the only difference between the kth approximation and the $(k-1)$th approximation is a single new basis, unlike a FVM approximation where upgrading to the kth approximation may involve finding a total of k new bases. For the SFA method, the coefficients c_d^j and interpolation functions $\psi_d^j(\mathbf{r})$, $j = 1, \ldots, k-1$, that form $\widetilde{I}_d^{k-1}(\mathbf{r})$ are held fixed while the coefficient c_d^k and interpolation function $\psi_d^k(\mathbf{r})$ are computed optimally according to some appropriate criterion, such as the minimization of an objective function Λ. Depending on the basis functions used, SFA should have access to popular adaptive grid methods.

There are no restrictions on the distribution of these bases and a broad class of basis functions can be used (e.g., low-order polynomials, B-splines, and radial basis functions). Since bases added later will change the computational mesh as needed, an h–r-type adaptive grid is created effectively, matrix-free, without the need for *a posteriori* error estimation and the associated remeshing. In addition, bases can be concentrated near high gradients or any other desired areas, provided the basis is chosen using that objective.

The dimensionality of the non-linear optimization problem is kept low by solving for only one basis (or at most a few bases) at a time. The weighted residual method is applied to define well-posed problems, and numerical stability issues are limited to the non-linear optimization process. Multiple processors may be devoted to finding the kth basis by using parallelizable optimization codes such as parallel direct search (PDS) [16]. Alternatively, an efficient sequential optimization method can be used with parallel evaluation of multiple bases (e.g., kth, $(k+1)$th and $(k+2)$th). Also, the algorithm can be initialized with either an empty set or an arbitrary number of predetermined functions and coefficients. The second option enables the use of solutions from a previous numerical analysis.

2.4. Formulation of the objective function

Each individual PDE of the DOM radiation problem can be written as

$$\mathcal{L}\big[I_d(\mathbf{r}), \mathbf{r}\big] = g_{\mathcal{L}}\big[\mathbf{I}(\mathbf{r}), I_d(\mathbf{r}), \mathbf{r}\big]$$

subject to the boundary conditions

$$\mathcal{B}\big[I_d(\mathbf{r}_B), \mathbf{r}_\mathrm{B}\big] = g_{\mathcal{B}}\big[\mathbf{I}(\mathbf{r}_\mathrm{B}), I_d(\mathbf{r}_\mathrm{B}), \mathbf{r}_\mathrm{B}\big]$$

The equation residual in each PDE and boundary condition may be determined after every stage of the SFA algorithm. Thus, after k SFA stages the residuals are

$$\mathbf{R}_{\mathcal{L}}^k(\mathbf{r}) = \left\{ \begin{array}{c} g_{\mathcal{L}}\big(\widetilde{\mathbf{I}}^k, \widetilde{I}_1^k, \mathbf{r}\big) - \mathcal{L}\big(\widetilde{I}_1^k, \mathbf{r}\big) \\ \vdots \\ g_{\mathcal{L}}\big(\widetilde{\mathbf{I}}^k, \widetilde{I}_D^k, \mathbf{r}\big) - \mathcal{L}\big(\widetilde{I}_D^k, \mathbf{r}\big) \end{array} \right\} \tag{3}$$

and

$$\mathbf{R}_{\mathcal{B}}^k(\mathbf{r}_\mathrm{B}) = \left\{ \begin{array}{c} g_{\mathcal{B}}\big(\widetilde{\mathbf{I}}^k, \widetilde{I}_1^k, \mathbf{r}_\mathrm{B}\big) - \mathcal{B}\big(\widetilde{I}_1{}^k, \mathbf{r}_\mathrm{B}\big) \\ \vdots \\ g_{\mathcal{B}}\big(\widetilde{\mathbf{I}}^k, \widetilde{I}_D^k, \mathbf{r}_\mathrm{B}\big) - \mathcal{B}\big(\widetilde{I}_D^k, \mathbf{r}_\mathrm{B}\big) \end{array} \right\} \tag{4}$$

The equation residuals of equations (3) and (4) are minimized by a fully coupled formulation without the need for an explicit source function, since all of the ordinate directions proceed simultaneously toward the correct solution with each additional SFA basis.

Using a geometric interpretation of the method of weighted residuals, the optimum basis for a given direction at the kth SFA stage can be determined from [11]

$$\min(\Lambda) = \min\left(-\left[\sum_{l=1}^{D} \langle \phi_{il}^k, \phi_{il}^k \rangle \right]^{-1} \sum_{j=1}^{D} \langle \mathbf{R}_j^{k-1}, \phi_{ij}^k \rangle^2 \right)$$
$$i = 1, \ldots, D \tag{5}$$

where, for notational convenience, the previous formulation was made with the assumption that the Dirichlet boundary conditions were satisfied. The boundary operator terms, therefore, are not shown, and the subscript $\mathcal{L}$ has been dropped from the vector of equation (3). The inclusion of boundary operators is straightforward. The coefficients are calculated from the Petrov–Galerkin method,

$$\sum_{j}^{D} \langle \mathbf{R}_j^k, \phi_{ij}^k \rangle = \mathbf{0}_i, \quad i = 1, \ldots, D \tag{6}$$

where the weighting function $\phi_{ij}^k \equiv \delta_{ij} \mathcal{L}(\psi_i^k)$ is used.

Since equation (5) uses the $(k-1)$th equation residual vector, the calculation of the weighting functions ϕ_{ij}^k (and thus, ψ_i^k) for a given direction is independent of the other ordinate directions. As a result, each component of equation (5) can be minimized independently and in parallel.

With the application of equation (6) to the radiative transfer equation the optimization problem can be written for each direction d as

$$\min(\Lambda) = \min\left(-\frac{A_d^2}{B_d}\right), \quad d = 1, \ldots, D \tag{7}$$

where, neglecting the parameters of the RTE for the sake of clarity,

$$A_d \equiv \sum_{j=1}^{k-1}\Bigg[\sum_{p=1}^{D} c_p^j\left(\langle\nabla\psi_d^k, \psi_p^j\rangle + \langle\psi_d^k, \psi_p^j\rangle\right) - c_d^j\left(\langle\nabla\psi_d^k, \nabla\psi_d^j\rangle + \langle\nabla\psi_d^k, \psi_d^j\rangle + \langle\psi_d^k, \nabla\psi_d^j\rangle + \langle\psi_d^k, \psi_d^j\rangle\right)\Bigg]$$

and $B_d \equiv \langle\nabla\psi_d^k, \nabla\psi_d^k\rangle + 2\langle\nabla\psi_d^k, \psi_d^k\rangle + \langle\psi_d^k, \psi_d^k\rangle$, $d = 1, \ldots, D$.

2.5. Boundary conditions

The optimization variables are the n_p parameters of the chosen basis ψ_d^k. The constraints on these parameters (**Q**), which the optimization routine must satisfy, depend on the form of the basis, the optimization method, and the original boundary conditions. In general, these constraints can be classified as the lower and upper bounds required to keep the basis finite for finite valued parameters and one constraint per dimension to satisfy the original boundary operator in the propagation direction.

The constraints for the lower and upper bounds may be unnecessary if the basis is well behaved. The latter type of constraint may be unnecessary if the boundary operator is incorporated into the objective function or if the basis automatically satisfies the boundary operator due to convenient parameter bounds.

2.6. Optimization methods

For speed and accuracy on a scalar computer a gradient-based optimization algorithm is needed. The gradient in basis parameter space of the objective function described in equation (7) is found as

$$\nabla\Lambda = -2\frac{A_d}{B_d}\nabla A_d + \left(\frac{A_d}{B_d}\right)^2\nabla B_d$$

and A_d, B_d, and Λ are all continuous in the parameter space. However, if piecewise continuous bases are chosen, ∇A_d and ∇B_d, and therefore $\nabla\Lambda$, will be discontinuous. This necessitates a non-smooth optimization routine. To date two such routines, SolvOpt [17] and FFSQP [18], have been used successfully by the authors. Of these two, SolvOpt showed better performance for our test cases and was used to generate the results presented in this text.

2.7. Basis functions

The choice of the proper form of the bases plays a major role in the efficiency of the algorithm as a whole and its utility. We chose local bases since the algorithm will have much greater utility applied to irregular problem domains. Arguably the most popular local basis is the piecewise linear B_1 spline ("hat function"), defined as

$$\psi_{\text{lin}}(x) \equiv \begin{cases} \dfrac{\eta + x_{\text{L}}}{x_{\text{L}}} & -x_{\text{L}} \le \eta \le 0 \\ \dfrac{\eta - x_{\text{R}}}{-x_{\text{R}}} & 0 < \eta \le x_{\text{R}} \\ 0 & \text{otherwise} \end{cases}$$

with local coordinate η is defined as

$$\eta(x) \equiv x - x_{\text{M}}$$

The constraints required for $\psi_{\text{lin}}(x)$ are

$$\mathbf{Q}_{\text{lin}} = \begin{bmatrix} x_{\text{L}} - \varepsilon_r \\ x_{\text{M}} \\ x_{\text{R}} - \varepsilon_r \\ 1 - x_{\text{M}} \\ \begin{cases} x_{\text{M}} - x_{\text{L}} & \Omega_d > 0 \\ 1 - x_{\text{M}} - x_{\text{R}} & \Omega_d < 0 \end{cases} \end{bmatrix} \ge 0$$

so $n_p = 3$.

Multi-dimensional bases can be formed from tensor products of the B_1, or $\psi_{\text{lin}}(x, y) \equiv \psi_{\text{lin}}(x)\psi_{\text{lin}}(y)$. Bases aligned with the x and y directions are limited in their ability to model discontinuities along an arbitrary direction with the SFA method. If one imagines the discontinuity as a boundary, then it is well known in finite elements that boundaries are better matched with elements that are properly aligned (e.g., unstructured grids) than with those that are not (e.g., structured grids).

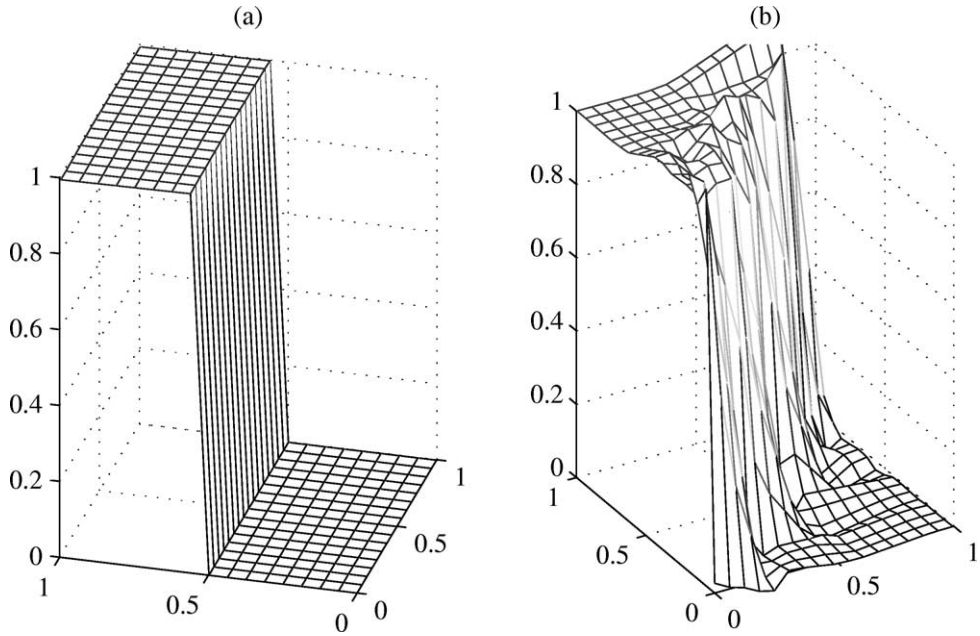

Figure 1. Bilinear sequential function approximation of discontinuity: (a) 1 basis, discontinuity aligned with coordinates; (b) 20 bases, discontinuity not aligned with coordinates.

Figure 1 illustrates that using the SFA method, an aligned boundary can be approximated with a single aligned basis. However, even after a large number of aligned bases are added with the SFA algorithm, a simple skewed boundary cannot be approximated.

In order to overcome this problem a skewed bilinear basis was developed that can have its local axes aligned in arbitrary directions. The form of the basis can be written as

$$\psi_{\text{skewed}}(x, y) = \psi_{\text{lin}}(\eta)\psi_{\text{lin}}(\xi)$$

where η and ξ are basis local coordinates defined such that

$$x = x_{\text{M}} + \eta\cos\theta_x - \xi\sin\theta_y \quad \text{and}$$
$$y = y_{\text{M}} + \eta\sin\theta_x + \xi\cos\theta_y$$

The skewed bases are centered at $(x_{\text{M}}, y_{\text{M}})$ as are the non-skewed variety. The constraints required for $\psi_{\text{skewed}}(x, y)$ are

$$\mathbf{Q}_{\text{skewed}} = \begin{bmatrix} \mathbf{Q}_{\text{lin}}(x) \\ \mathbf{Q}_{\text{lin}}(y) \\ \theta_x \\ \theta_y \end{bmatrix} \geq 0$$

so $n_p = 8$. Note that we can recover the aligned bilinear basis when $\theta_x = \theta_y = 0$. *Figure 2* illustrates that the SFA algorithm can now accurately approximate both an aligned and a non-aligned discontinuity using only a single skewed basis function.

Unfortunately, with skewed bases, inner products of the form $\langle\psi^i(x, y), \psi^j(x, y)\rangle$ cannot be evaluated as $\langle\psi^i(x), \psi^j(x)\rangle \cdot \langle\psi^k(y), \psi^l(y)\rangle$ since local basis coordinates η and ξ are no longer orthogonal. This concern can be addressed by breaking the bases down into quadrants. Since x and y are linear functions of η and ξ, each basis is in effect a quadratic function of x and y. Thus, the product of two basis (within a quadrant) is a fourth-order polynomial of x and y (at most). The resultant quadrants may then be decomposed into discrete two-dimensional triangular elements, over which standard six-point Gauss quadrature rules may be used to integrate fourth-order polynomials exactly.

3. RESULTS

The two-dimensional problem investigated consists of radiative heat transfer between four sides of an $L \times L$ square black box as shown in *figure 3* filled with an isotropically scattering medium. The medium is at radiative equilibrium and has an extinction coefficient of β. Isothermal conditions were maintained on all surfaces.

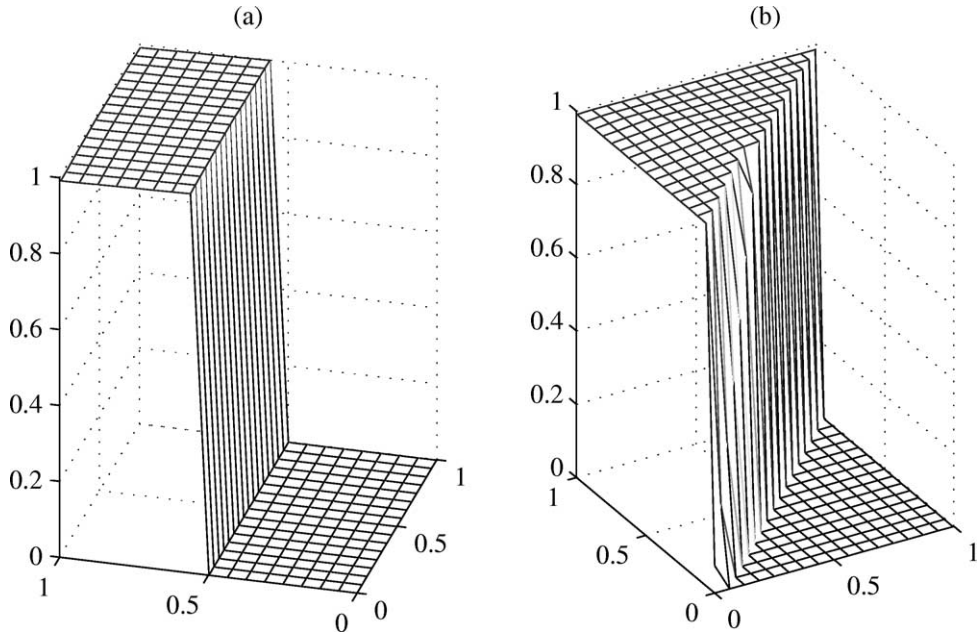

Figure 2. Skewed bilinear sequential function approximation of discontinuity: (a) 1 basis, discontinuity aligned with coordinates; (b) 1 basis, discontinuity not aligned with coordinates.

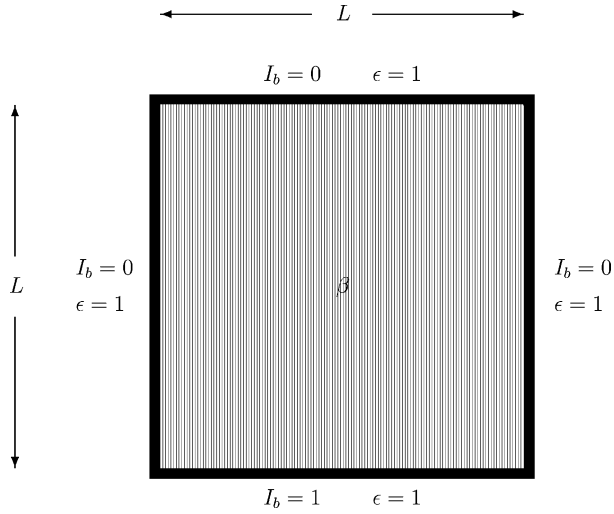

Figure 3. Radiation in a square black box.

The resulting dimensionless intensity leaving the three cold walls was $I_b = 0$ with $I_b = 1$ at the remaining wall; all four surfaces are black ($\varepsilon = 1$).

Following the procedure outlined in Section 2, the two-dimensional DOM/RTE was solved by the SFA method using the SolvOpt optimization algorithm combined with the skewed bilinear bases. The SolvOpt optimization package (version 1.1 with default parameters and constraint tolerance set to zero) was used for the optically thin and thick S_2 and the optically medium S_6 cases shown in *figures 4–11*. The boundary conditions of the physical problem were satisfied by initial bases. Subsequent bases were constrained so that their values were zero at the boundaries. Ordinate directions were selected and subsequent bases were placed randomly along each of the ordinates with their local axes initially aligned with the global x and y (i.e., initialization of the optimization variables). These bases then altered location, width, and orientation, with respect to the global axes, to minimize the equation residual without user intervention. The incident radiation and heat flux scalar were computed from

$$\frac{G}{4\pi} = \sum_{d=1}^{D} w_d I_d \quad \text{and} \quad \frac{q}{\pi} = \sum_{d=1}^{D} w_d \Omega_{dn} I_d$$

respectively. SFA results were compared to FVM solutions using the diamond and step schemes on a regular grid. All calculations were made on a SUN Ultra 1 using a 143 MHz floating point processor. As *figures 4–11* indicate, the SFA algorithm provides more accurate solutions with far fewer bases than the CVs used in the conventional FVMs.

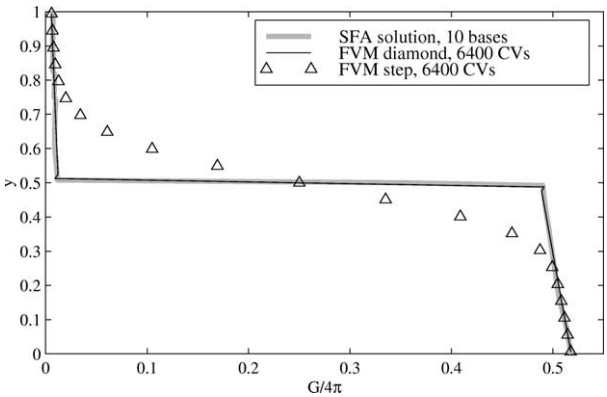

Figure 4. DOM solutions for incident radiation G along the centerline ($x = 0.5$, $L = 1$), thin medium: S_2, $\beta = 0.1$.

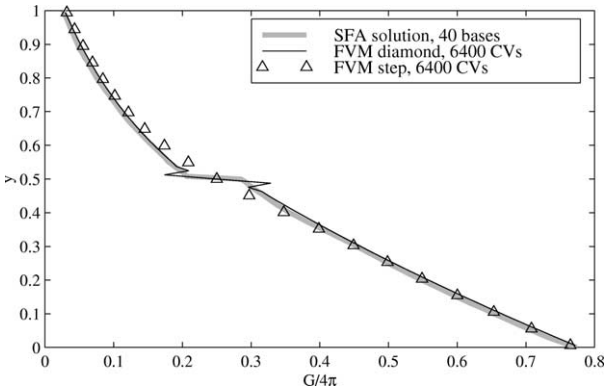

Figure 5. DOM solutions for incident radiation G along the centerline ($x = 0.5$, $L = 1$), thick medium: S_2, $\beta = 3.0$.

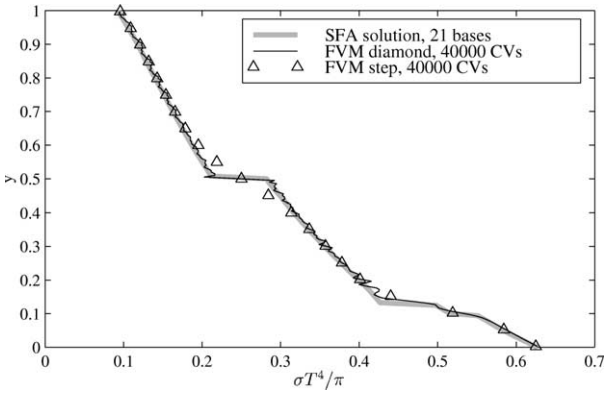

Figure 6. Solution of centerline temperature by SFA, FVM diamond, and FVM step schemes: S_6, $\beta = 1.0$, $L = 1$.

One of the more interesting results of the multi-dimensional SFA algorithm is the ability to minimize the effect of artificial scattering so that discontinuities are

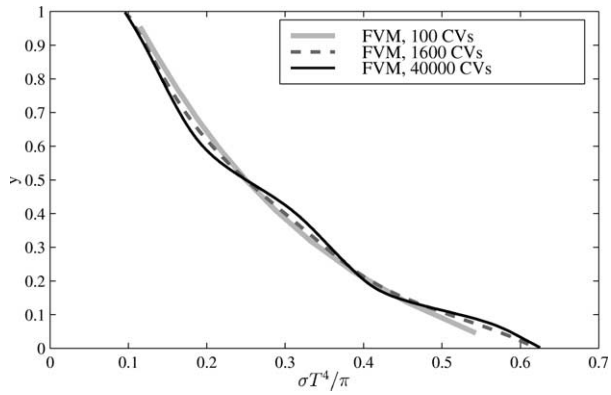

Figure 7. Grid dependent FVM step scheme solution of centerline temperature: S_6, $\beta = 1.0$, $L = 1$.

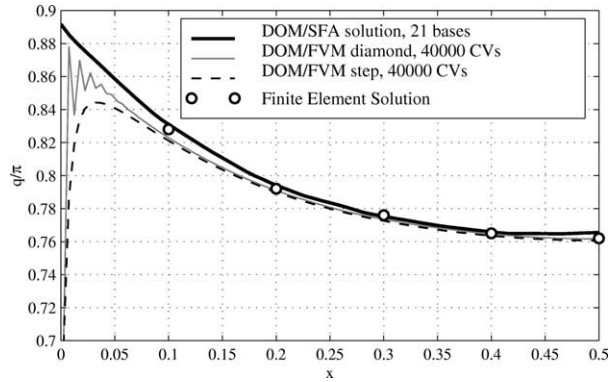

Figure 8. Non-dimensional heat flux along hot wall: S_6, $\beta = 1.0$, $L = 1$.

matched without smearing or oscillations, as illustrated in *figures 4–6*. The SFA algorithm does so with fewer than 1 % of the number of FVM control volumes.

As mentioned in Section 1, solutions enhanced by artificial scattering such as those of the FVM step scheme have questionable validity. To illustrate this, a grid dependent centerline temperature profile is given in *figure 7*. Increasing the number of CVs leads to a less smooth solution as the artificial scattering is reduced and the discontinuities are better approximated. From these results it is seen that the standard practice of choosing a grid density that will give results that best match a published solution can be misleading.

The artificial scattering in FVM solutions also affects the heat flux calculations. *Figure 8* compares the symmetric heat flux along one half of the bottom wall from the SFA, FVM diamond, and FVM step scheme using the DOM/RTE to a finite element solution [19] of the full RTE. It is noted that near the corners of the box the FVM solutions diverge dramatically from the expected

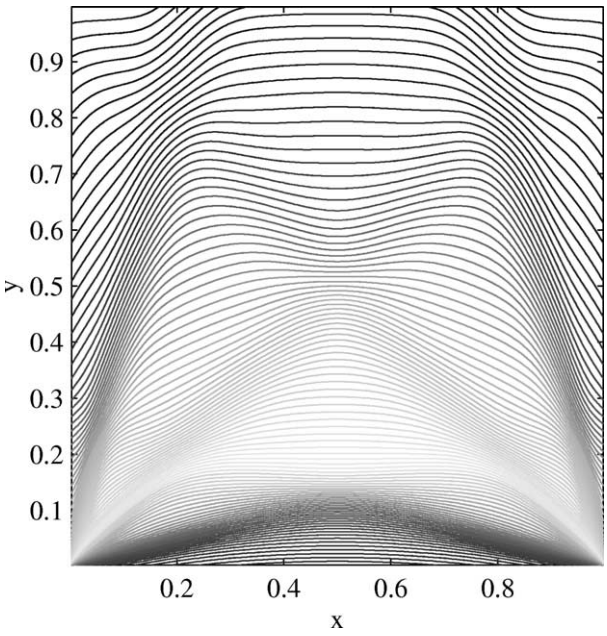

Figure 9. Non-dimensional temperature, FVM step scheme: S_6, $\beta = 1.0$, 40 000 control volumes, $L = 1$.

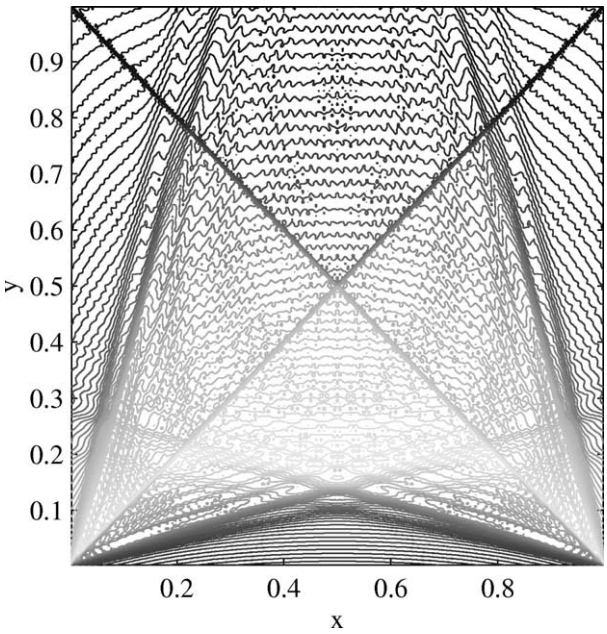

Figure 10. Non-dimensional temperature, FVM diamond scheme: S_6, $\beta = 1.0$, 40 000 control volumes, $L = 1$.

heat flux profiles. To overcome this problem, the heat flux is typically not reported near the corner (e.g., results shown by Modest [20] and Ramankutty and Crosbie [21]) or the solution is extrapolated to the corner by some other means. The SFA solution, however, gives consistently smooth heat flux predictions along the entire hot wall without oscillations or extrapolation.

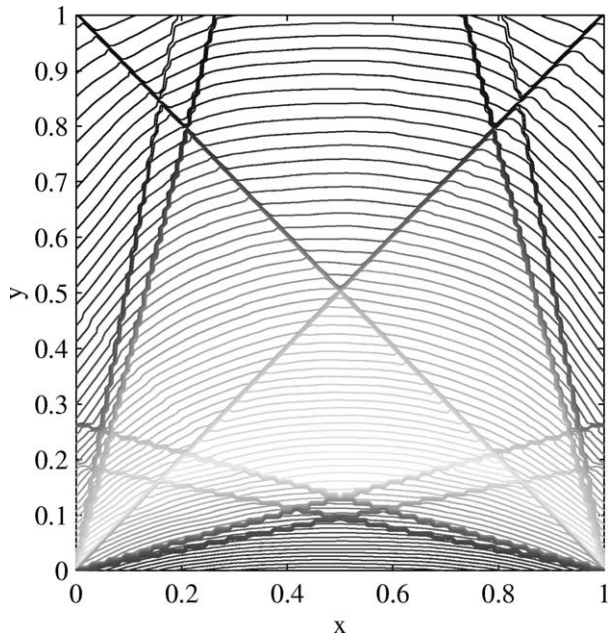

Figure 11. Non-dimensional temperature, SFA method: S_6, $\beta = 1.0$, 21 bases, $L = 1$.

To further illustrate the SFA method's stability and reduction of artificial scattering, the non-dimensional temperature distributions are shown for the problem domain in *figures 9–11*. The contours show high (bottom of domain) to low (top of domain) values of non-dimensional temperature. *Figure 9* shows how the FVM step scheme smears the discontinuities through false scattering and also smooths the solution between the discontinuities. In *figure 10* we see that the FVM diamond scheme models the discontinuities fairly well, as evidenced by the presence of discrete rays in the approximation. But we also notice that the discontinuities are still smeared, albeit slightly, by the artificial scattering. More importantly the non-dimensional temperature, which should vary smoothly between these rays, is oscillatory.

The non-dimensional temperature distribution calculated by the SFA method is illustrated in *figure 11*. Here the discontinuities are crisp and distinct throughout the domain. Also, the non-dimensional temperature distribution between the discontinuities is smooth. The angles of these rays correspond precisely to the discrete ordinate directions chosen. Note that while the FVM scheme requires 40 000 CVs, the SFA result requires only 21 skewed bilinear bases. In other words, the number of

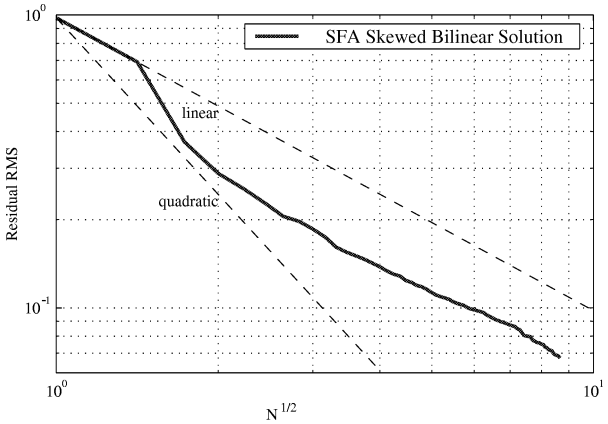

Figure 12. Convergence history: S_6, $\beta = 1.0$, $L = 1$.

bases that the SFA method requires is only 0.05 % of the number CVs used in the FVM.

Using the convergence rate (RMS versus $N^{1/\zeta}$) to measure the performance of the SFA algorithm, we note that with the RMS of the equation residual,

$$\text{RMS} \leq \|\varepsilon_r\|_{H^1}$$

Figure 12 for S_6 and $\beta = 1.0$ displays the significant performance benefits the SFA method provides compared to the conventional FVM. Because the B_1 spline and FVM control volume are piecewise linear and the solution is linear, then $p = 1$, $m = 1$, and $s = 1$ in equation (1). Therefore, using a non-linear optimization routine, the B_1 spline and control volume should approach an optimal convergence rate of $\gamma = 1$ with increasing $N^{1/\zeta}$. The initial quadratic (or higher) convergence for the S_6 and $\beta = 1.0$ case of *figure 12* is caused by the relocation component of the SFA [22] since it places the bases where they will reduce the equation residual the greatest. This is most effective with the first few bases. The convergence rate should approach the theoretical optimum predicted by error analysis for B_1 splines as N increases further. This is evident in *figure 12* for $N > 4$. This convergence study proves that the SFA method does not adversely affect the optimal convergence rate of B_1 splines. As a result, we judge the application of SFA to the two-dimensional DOM/RTE with skewed bilinear bases to be successful.

4. CONCLUSIONS

The SFA method [22] may prove to be an attractive adaptive and scalable alternative to the FE and FVM approaches in the efficient solution of the multi-dimensional DOM/RTE. The developed algorithm is a user-friendly, solution-adaptive, and matrix-free automatic meshless solver. SFA solutions to the problem of heat transfer within a two-dimensional box through a non-scattering medium have been presented and compared to the results from a conventional DOM/FVM. The accuracy level of the SFA results using skewed local bases clearly surpasses the FVM results using the popular step and diamond schemes on a regular grid. More importantly, the SFA accuracy levels are achieved with far fewer low-order bases. In its worst case, the required SFA bases are fewer than 1 % of the number of CVs used by the FVM schemes and in its best case only 0.05 %. From a numerical analysis perspective, one of the SFA method's attractive features is that its convergence rate is no less than, and can initially exceed, the theoretical optimum for the piecewise linear bases.

Acknowledgements

Support for this work was provided by the Office of Naval Research grant N00014-95-1-0741 under Dr. Thomas McKenna. The authors are grateful to Franz Kappel for the use of the SolvOpt optimization package.

REFERENCES

[1] Howell J.R., Thermal radiation in participating media: the past, the present, and some possible futures, J. Heat Tran. 110 (1988) 1220–1229.

[2] Celmaster W., May E.N., Parallelization of a radiation transport simulation code on the BBN TC2000 parallel computer, in: Proceedings of Supercomputing 1990, ASME Press, 1990, pp. 448–454.

[3] Novo P.J., Coelho P.J., Carvalho M.J., Parallelization of the discrete transfer method: two different approaches, in: National Heat Transfer Conference, Vol. 3, HTD, Vol. 325, ASME Press, 1996, pp. 45–54.

[4] Fiveland W.A., Discrete-ordinates solutions of the radiative transport equation for rectangular enclosures, J. Heat Tran. 106 (1984) 699–706.

[5] Wang Y., Bayazitoglu Y., Wavelets and discrete ordinates method in solving one-dimensional nongray radiation problem, Int. J. Heat Mass Tran. 42 (1999) 385–393.

[6] Fiveland W.A., The selection of discrete ordinate quadrature sets for anisotropic scattering, in: Fundamentals of Radiation Heat Transfer, Vol. 160, ASME Press, 1991, pp. 89–96.

[7] Haferman J.L., Smith T.F., Krajewski W.F., Multi-dimensional radiative transfer computation using scalable parallel implementation of the discrete-ordinates method, in: Proceedings of the 1994 International Geoscience and Remote Sensing Symposium, Vol. 3, 1994, pp. 1623–1625.

[8] Burns S.P., Application of spatial and angular domain based parallelism to a discrete ordinates formulation

with unstructured spatial discretization, in: Proceedings of Second International Symposium on Radiation Transfer, International Centre for Heat and Mass Transfer, Kusadasi, Turkey, 1997, pp. 173–193.

[9] Chai J.C., Lee H.S., Patankar S.V., Ray effect and false scattering in the discrete ordinates method, Numer. Heat Tran. B 24 (1993) 373–389.

[10] Hirsch C., Numerical Computation of Internal and External Flows, Vol. 2, Wiley, New York, 1990.

[11] Meade A.J., Kokkolaras M., Zeldin B.A., Sequential function approximation for the solution of differential equations, Comm. Numer. Methods Engrg. 13 (1997) 977–986.

[12] Diaz A.R., Kikuchi N., Taylor J.E., A method of grid optimization for finite element methods, Comput. Methods Appl. Mech. Engrg. 41 (1983) 29–45.

[13] Johnson C., Numerical Solution of Partial Differential Equations by the Finite Element Method, Cambridge University Press, New York, 1990.

[14] Eiseman P.R., Choo Y.K., Smith R.E., Algebraic grid generation with control points, in: Chung T.J. (Ed.), Finite Elements in Fluids, Vol. 8, Hemisphere, Washington, 1992.

[15] Oden J.T., Adaptive methods in computational fluid dynamics, in: Chung T.J. (Ed.), Finite Elements in Fluids, Vol. 8, Hemisphere, Washington, 1992.

[16] Dennis J.E., Torczon V., Direct search methods on parallel machines, SIAM J. Opt. 1 (1991) 448–474.

[17] Kuntsevich A., Kappel F., SolvOpt: the solver for local nonlinear optimization problems, Institute for Mathematics, Karl-Franzens University of Graz, 1997.

[18] Zhou J.L., Tits A.L., Lawrence C.T., User's guide for FFSQP version 3.7: a Fortran code for solving constrained nonlinear (minimax) optimization problems, generating iterates satisfying all inequality and linear constraints, Electrical Engineering Department and Institute for System Research, University of Maryland, 1997.

[19] Razzaque M.M., Klein D.E., Howell J.R., Finite element solution of radiative heat transfer in a two-dimensional rectangular enclosure with gray participating media, J. Heat Tran. 105 (1983) 933–936.

[20] Modest M.F., Radiative Heat Transfer, McGraw-Hill, New York, 1993.

[21] Ramankutty M.A., Crosbie A.L., Modified discrete ordinates solution of radiative transfer in two-dimensional rectangular enclosures, J. Quant. Spectrosc. Radiat. Tran. 57 (1997) 107–140.

[22] Thomson D.L., Meade A.J., Bayazitoglu Y., The development of a sequential function approximation solution to the radiative transfer equation, Thermal Sci. Engrg. 8 (2000) 9–18.